JACS
JOURNAL OF THE AMERICAN CHEMICAL SOCIETY
Article
pubs.acs.org/JACS

$Ag_{50}(Dppm)_6(SR)_{30}$ and Its Homologue $Au_xAg_{50-x}(Dppm)_6(SR)_{30}$ Alloy Nanocluster: Seeded Growth, Structure Determination, and Differences in Properties

Wenjun Du,[†] Shan Jin,[†] Lin Xiong,[‡] Man Chen,[†] Jun Zhang,[§] Xuejuan Zou,[†] Yong Pei,[‡] Shuxin Wang,*[,†] and Manzhou Zhu*[,†]

[†]Department of Chemistry and Center for Atomic Engineering of Advanced Materials, Anhui University, Hefei, Anhui 230601, PR China

[‡]Department of Chemistry, Key Laboratory of Environmentally Friendly Chemistry and Applications of Ministry of Education, Xiangtan University, Xiangtan, Hunan 411105, PR China

[§]School of Materials and Chemical Engineering, Anhui Jianzhu University, Hefei, Anhui 230601, PR China

Supporting Information

ABSTRACT: A large thiolate/phosphine coprotected $Ag_{50}(Dppm)_6(SR)_{30}$ nanocluster was synthesized through the further growth of $Ag_{44}(SR)_{30}$ nanocluster and characterized by X-ray photoelectron spectroscopy (XPS), electrospray ionization mass spectrometry (ESI-MS), and single-crystal X-ray analysis. This new nanocluster comprised a 32-metal-atom dodecahedral kernel and two symmetrical $Ag_9(SR)_{15}P_6$ ring motifs. The 20 valence electrons correspond to shell closure in the Jellium model. Moreover, this nanocluster could be alloyed by templated/galvanic metal exchange to the homologue $Au_xAg_{50-x}(Dppm)_6(SR)_{30}$ nanocluster; the latter showed much higher thermal stability than the $Ag_{50}(Dppm)_6(SR)_{30}$ nanocluster. Further experiments were conducted to study the optical, electrical, and photoluminescence properties of both nanoclusters. Our work not only reports two new larger size nanoclusters but also reveals a new way to synthesize larger size silver and alloy nanoclusters, that is, controlled growth/alloying.

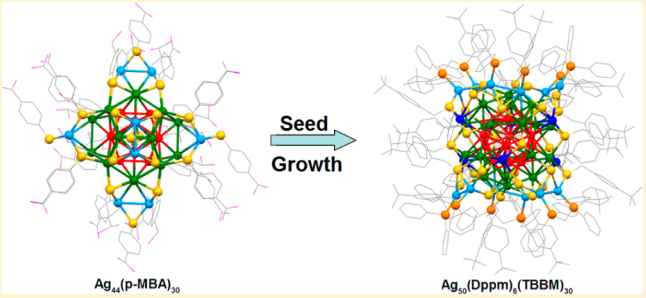

1. INTRODUCTION

Noble metal nanoclusters (size <2 nm) have attracted great research attention for their unique properties. In this ultrasmall size range, nanoclusters lose the plasmonic features and show molecular properties.[1,2] Determination of nanocluster structure gives the possibility to study their related properties, especially for the larger ones which are the most appealing for many fields.[3−5] In the past years, a series of homogold nanoclusters were synthesized and structurally characterized by X-ray crystallography, including Au_{18},[6,7] Au_{20},[8,9] Au_{21},[10] Au_{22},[11] Au_{23},[12] Au_{24},[13−15] Au_{25},[16−18] Au_{28},[19−21] Au_{30},[22,23] Au_{36},[24,25] Au_{37},[26] Au_{38},[27] Au_{40},[28] Au_{44},[29] Au_{52},[28] Au_{92},[30] Au_{102},[31,32] Au_{130},[33] and Au_{133}.[34,35] With the well-defined structures, the related properties can be achieved and utilized for various applications, including catalysis,[36−38] bioapplication,[39−41] photochemistry,[42−46] magnetism,[47,48] and energy conversion.[49,50]

Complex ligand exchange was found to be an efficient way to alter the size of gold nanoclusters,[51−53] i.e., by using thiol ligand reacted with phosphine and halide coprotected Au_{11} nanocluster multiligands protected $Au_{25}(PPh_3)_{10}(SR)_5Cl_2$ or $Au_{37}(PPh_3)_{10}(SR)_{10}Cl_2$ nanocluster could be synthesized.[26,54] However, study on complex ligand exchange in thiolated silver nanocluster was relatively rare.

The thiolated silver nanocluster $Ag_{44}(SR)_{30}^{4-}$ was reported by using *p*-mercaptobenzoic acid (*p*-MBA) and fluorinated arylthiols ligands, respectively.[55−58] This nanocluster showed an ultrastable nature and could be synthesized at large scale, which provided an ideal model for complex ligand exchange reaction.

Herein we present a complex ligand exchange method to achieve the controlled growth for larger size Ag_{50} nanocluster by using Ag_{44} as seeds (for details, see the Experimental Section). This new nanocluster has an overall composition of $Ag_{50}(Dppm)_6(SR)_{30}$ with the 50 metal atoms distributed in a $Ag_{12}@Ag_{20}@Ag_6@Ag_{12}$ distribution. The structure comprises a Ag_{32} kernel (a hollow icosahedron (Ag_{12}) which is retained from Ag_{44} surrounded by a dodecahedron (Ag_{20})) and two symmetrical $Ag_9(SR)_{15}P_6$ ring motifs. The $Ag_{50}(Dppm)_6(SR)_{30}$ nanocluster has a C_{3i} point group, with free valence electrons counted to be 20 ($n_s = 50 - 30 - 0 = 20$), which is a closed shell Jellium number. In order to make the structure more stable, we have applied the "templated/galvanic metal exchange" method[59,60] to dope the inert gold atoms into the Ag metal core and accordingly obtained the homologue

Received: November 10, 2016
Published: January 23, 2017

DOI: 10.1021/jacs.6b11681
J. Am. Chem. Soc. 2017, 139, 1618−1624

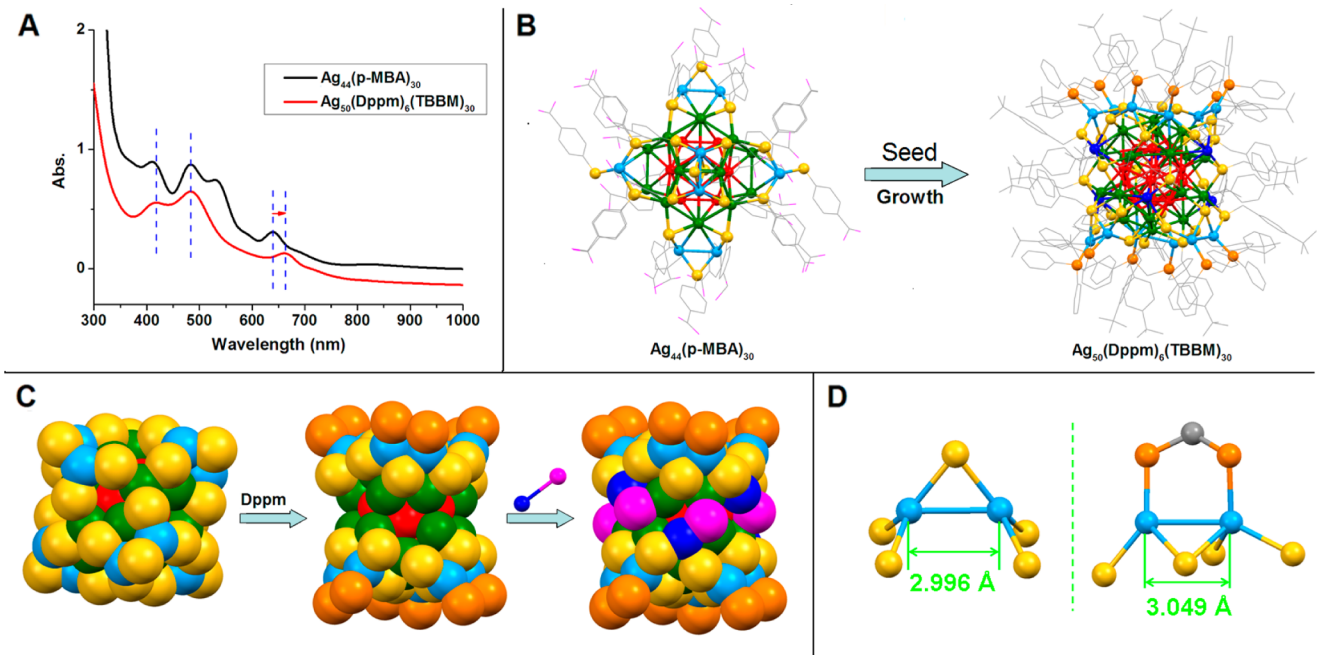

Figure 1. (A) Comparison of the UV−vis between Ag_{44} and Ag_{50}. (B) Total crystal structures transform from the $Ag_{44}(p\text{-MBA})_{30}$ to the $Ag_{50}(Dppm)_6(SR)_{30}$ nanocluster. (C) Schematic diagram of the conversion from the Ag_{44} and Ag_{50}. (D) Comparison of the structures of different surface staple units between Ag_{44} and Ag_{50} (color labels: red/green/blue/sky blue = Ag; yellow/magenta = S; orange = P; gray = C; violet = O. For clarity, all H atoms are not shown.

$Au_{5.34}Ag_{44.66}(Dppm)_6(SR)_{30}$ alloy nanocluster (for details of occupancy, please see the Supporting Information). The atomic compositions of these two nanoclusters were further confirmed by XPS. Ultraviolet−visible (UV−vis), photoluminescence, and electrochemical analyses were carried out to find the differences between these two nanoclusters.

2. EXPERIMENTAL SECTION

2.1. Chemicals. All reagents and solvents were commercially available and were used as received without further purification, including tetrachloroauric(III) acid ($HAuCl_4{\cdot}3H_2O$, ≥99% metals basis), silver nitrate ($AgNO_3$, ≥98% metals basis), *p*-mercaptobenzoic acid (*p*-MBA, ≥99%), cesium hydroxide (CsOH, 50% w/w aqueous, Alfa-016505), 4-*tert*-butylbenzyl mercaptan ($HSCH_2Ph$-*t*-Bu, ≥99%), bis(diphenylphosphino)methane (Dppm, 98%), sodium borohydride ($NaBH_4$, 99%),sodium cyanoborohydride ($NaBH_3CN$, 99%), methanol (HPLC-grade, 99%), ethanol (HPLC-grade, 99%), dichloromethane (HPLC-grade, 99.9%), toluene (HPLC-grade, 99%), and hexane (HPLC-grade, 99.9%). Pure water was from Wahaha Co Ltd. All glassware was thoroughly cleaned with aqua regia (HCl/HNO_3 = 3:1 v/v), rinsed with plenty of pure water, and then dried in an oven prior to use.

2.2. Synthesis of $Ag_{44}(p\text{-MBA})_{30}$ Clusters. This nanocluster was synthesized by a reported method.[57] Briefly, $AgNO_3$ (42.5 mg) was dissolved in 21 mL of water under vigorous stirring. Then, 154 mg of *p*-MBA ethanolic solution was added to the $AgNO_3$ solution. The pH was then adjusted to 12 with CsOH to stabilize the final cluster product. After that, 9 mL of $NaBH_4$ aqueous solution (11 mg/mL) was added dropwise under vigorous stirring. The reaction was aged for ∼1 h at room temperature, and the dark red solution was the crude product of $Ag_{44}(p\text{-MBA})_{30}$. The clusters were separated from the reaction mixture by precipitation with ethanol and the dark red precipitate was collected by centrifugation (3 min at ∼10 000 rpm). The dark red precipitate was washed with excess ethanol and collected by centrifugation.

2.3. Seeded Growth/Ligand Exchange Method for the Synthesis of $Ag_{50}(Dppm)_6(SR)_{30}$ Clusters. First, 35 mg of $Ag_{44}(p\text{-MBA})_{30}$ clusters (powder) were added to a flask; then, 10 mL of methanol containing $AgNO_3$ (30 mg), Dppm (25 mg), and $HSCH_2Ph$-*t*-Bu (TBBM, 50 uL) were added under vigorous stirring. After that, 2 mL of $NaBH_3CN$ methanol solution (26 mg/mL) was added under vigorous stirring. The reaction was aged for ∼18 h at room temperature, and the supernatant was collected by centrifugation (3 min at ∼10 000 rpm) and then dried. The black product was washed with excess toluene and collected by centrifugation again. Black diamond-shaped crystals were crystallized from CH_2Cl_2/toluene at room temperature.

2.4. Synthesis of $Au_xAg_{50-x}(Dppm)_6(SR)_{30}$ Clusters. $Ag_{50}(Dppm)_6(SR)_{30}$ was dissolved in methanol under vigorous stirring. Then, Au(I)-SR (SR = TBBM) was added. After about 4 h, the peak of Ag_{50} (∼660 nm) was gradually blue shift to 616 nm, which indicates the exchange of gold atoms into the silver nanocluster. The supernatant was collected by centrifugation (3 min at ∼10 000 rpm) and then dried. The black product was washed with excess toluene and collected by centrifugation again. Black diamond-shaped crystals were crystallized from CH_2Cl_2/toluene at room temperature.

2.5. X-ray Crystallographic Determination. The data collections for single crystal X-ray diffraction (SCXRD) was carried out on a Bruker Smart APEX II CCD diffractometer at 150 K, using a graphite-monochromated Mo Kα radiation (λ = 0.71073 Å). Data reductions and absorption corrections were performed using the SAINT and SADABS programs, respectively. The structure was solved by direct methods and refined with full-matrix least-squares on F^2 using the SHELXTL software package. All non-hydrogen atoms were refined anisotropically, and all the hydrogen atoms were set in geometrically calculated positions and refined isotropically using a riding model. X-ray diffraction data refinement involving partial occupancy was used to locate the Au atom in $Au_{5.34}Ag_{44.66}(Dppm)_6(SR)_{30}$ (for details, see the Supporting Information).

2.6. DFT Calculations. The density functional theory (DFT) calculations were employed to optimize the geometric structure of $Ag_{50}(Dppm)_6(SR)_{30}$ and $Au_6Ag_{44}(Dppm)_6(SR)_{30}$ clusters using Perdew−Burke−Ernzerhof (PBE)[61] function, and the d-polarization included basis set (DND) is used for C, H, S, and P. The DFT Semicore pseudopotential (DSPP) approximation with some degree of relativistic corrections into the core is used for the Au and Ag

DOI: 10.1021/jacs.6b11681
J. Am. Chem. Soc. 2017, 139, 1618−1624

elements implemented in the Dmol^3 package.[62,63] (Here, the R group is simplified as methyl group to simplify the calculation.)

2.7. Characterization. Ultraviolet−visible (UV−vis) absorption spectra were recorded on Agilent 8453 spectrophotometer. Single crystals were dissolved in methanol for spectral measurements.

X-ray photoelectron spectroscopy (XPS) measurements were performed on Thermo ESCALAB 250. configured with a monochromated Al Kα (1486.8 eV) 150 W X-ray source, 0.5 mm circular spot size, a flood gun to counter charging effects, and the analysis chamber base pressure lower than 1×10^{-9} mbar; data were collected with FAT = 20 eV.

Electrochemical measurements of clusters were performed with an electrochemical workstation (CHI 700E) using a Pt working electrode (diameter 0.4 mm), a Pt wire counter electrode and an Ag wire quasi-reference electrode in 0.1 M Bu_4NPF_6−CH_2Cl_2. Prior to use, the working electrode was polished with 0.05 mg mL^{-1} Al_2O_3 slurries and then cleaned by sonication in dilute CH_3CH_2OH and nanopure water successively. The electrolyte solution was deaerated with ultrahigh purity nitrogen for 40 min and blanketed under a nitrogen atmosphere during the entire experimental procedure.

Photoluminescence spectra were measured on a FL-4500 spectrofluorometer with the same optical density (OD) ≈ 0.05. In these experiments, the nanoclusters solution was prepared in CH_2Cl_2 at a concentration of less than 1 mg mL^{-1}.

Electrospray ionization mass spectrum (ESI-MS) was recorded using a Bruker Q-TOF mass spectrometer. The source temperature was kept at 80 °C. The sample was directly infused into the chamber at 5 μL/min. To prepare the ESI sample, clusters were dissolved in methanol (~0.1 mg/mL).

3. RESULTS AND DISCUSSION

3.1. Crystal Structure. The UV−vis absorption spectra of $Ag_{44}(SR)_{30}$ nanocluster showed obvious peaks at ~410, 485, 530, and 640 nm and a weak broad peak at ~810 nm. After growth, $Ag_{50}(Dppm)_6(SR)_{30}$ displayed three obvious peaks at ~415, 485, and 660 nm; the broad peak was further widened (Figure 1A). The similar UV−vis spectra revealed that these two nanoclusters might have a similar structure. X-ray crystallography analysis was performed and found that the structure of Ag_{50} had an exceptionally high symmetry with C_{3i} point group (S_6 symmetry) (Figure S1). The symmetry was attributed to the six "S−Ag−S" staples which formed a hexagonal prism and occupied the interlaced vertices (Figure S1C). As shown in Figure 1B, the hollow Ag_{12} unit from Ag_{44} was maintained in the Ag_{50} nanocluster. Detailed analysis of the crystal structures of Ag_{44} and Ag_{50} revealed that the 12 Ag atoms in the motifs of Ag_{44} nanocluster were distributed at the 12 sides of the dodecahedron while the 12 Ag atoms in the motifs of Ag_{50} were scattered in the dodecahedron at the top of the six surfaces because every two Ag atoms were connected by a Dppm ligand (Figure 1B). The exchange of Dppm ligand and thiol resulted in enough space in the middle of Ag_{50} for the six Ag−S units to connect with the Ag_{32} kernel (Figure 1C). The Dppm ligand made the Ag_2S_4 distorted and stretched the Ag−Ag bond from 2.996 Å in Ag_{44} to 3.049 Å in Ag_{50} (Figure 1D). Furthermore, the six special Ag atoms were connected with the center Ag_{12} kernel and converted the six separate $Ag_2S_4P_2$ motifs to two ring-shaped motifs (Figure S2).

The details of the atom-packing structure were shown in Figure 2. The Ag_{50} nanocluster consisted of a hollow icosahedron (Ag_{12} inner core) (Figure 2A) within a dodecahedron (Ag_{20} outer core) (Figure 2B), forming an Ag_{32} excavated-dodecahedral core (Figure 2C) with icosahedral symmetry. Compared with the reported $Ag_{44}(SR)_{30}$ nanocluster, this newly formed nanocluster had 6 extra $Ag(SR)_2$ units (Figure 2E) which connected the independent

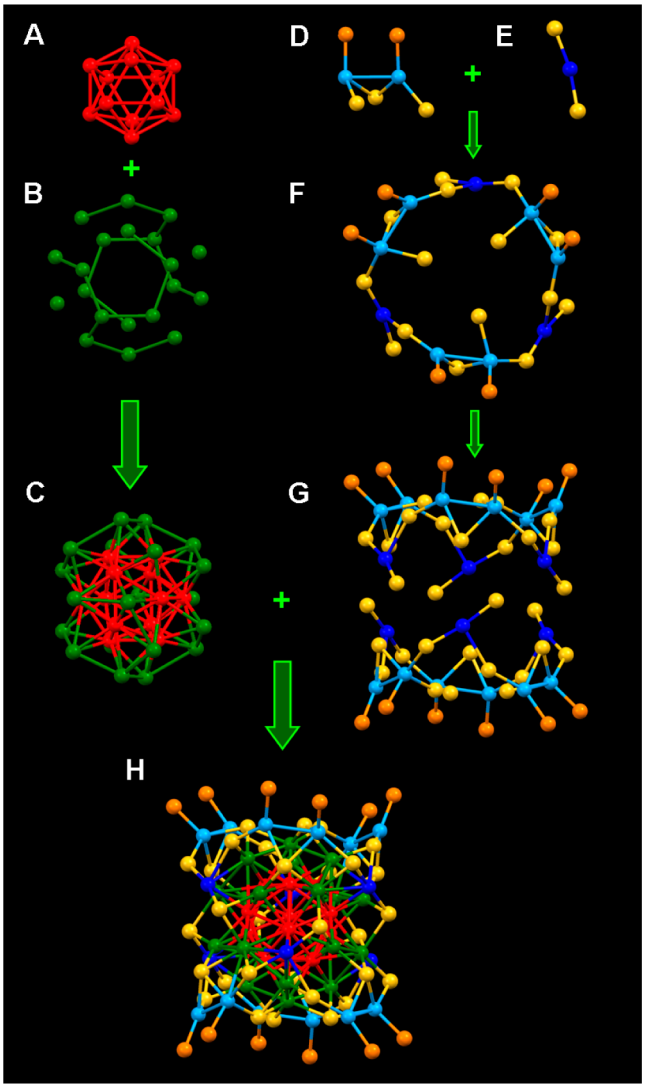

Figure 2. Dissected structure of $Ag_{50}(Dppm)_6(SR)_{30}$. Color labels: red/green/blue/sky blue = Ag; yellow = S; orange = P. For clarity, all C and H atoms are not shown.

$Ag_2(SR)_3(Dppm)_1$ units (Figure 2D) and accordingly formed two $Ag_9(Dppm)_3(SR)_{15}$ rings (Figure 2G). Meanwhile, these extra $Ag(SR)_2$ units connected the outside shell with both Ag_{12} kernel (Figure S2) and dodecahedron Ag_{20} outer core and finally formed the $Ag_{50}(Dppm)_6(SR)_{30}$ nanocluster (Figure 2H).

Due to the influence of dual ligands, the mount structure in Figure 2D comprised the entire layer protecting the compact, quasi-spherical Ag_{32} core. The radial Ag−Ag distances (2.786−2.871 Å) in the hollow icosahedron Ag_{12} were different from the Ag−Ag distances (2.813−2.843 Å) of the empty icosahedron Ag_{12} in $[Ag_{44}(p\text{-MBA})_{30}]^{4-}$ and shorter than the Ag−Ag distances (2.900−3.202 Å) in the dodecahedron (Ag_{20} outer core).[57]

Similar to most of the reported Ag nanoclusters, Ag_{50} was not very stable at higher temperature (Figure S4). To enhance the stability of this nanocluster, we used the templated/galvanic metal exchange method to dope inert Au atoms into this nanocluster. The $Au_{5.34}Ag_{44.66}(Dppm)_6(SR)_{30}$ cluster was obtained by adding Au(I)−SR complex into the Ag_{50} solution (Figure 3A). SCXRD revealed that gold atoms exchanged the

DOI: 10.1021/jacs.6b11681
J. Am. Chem. Soc. 2017, 139, 1618−1624

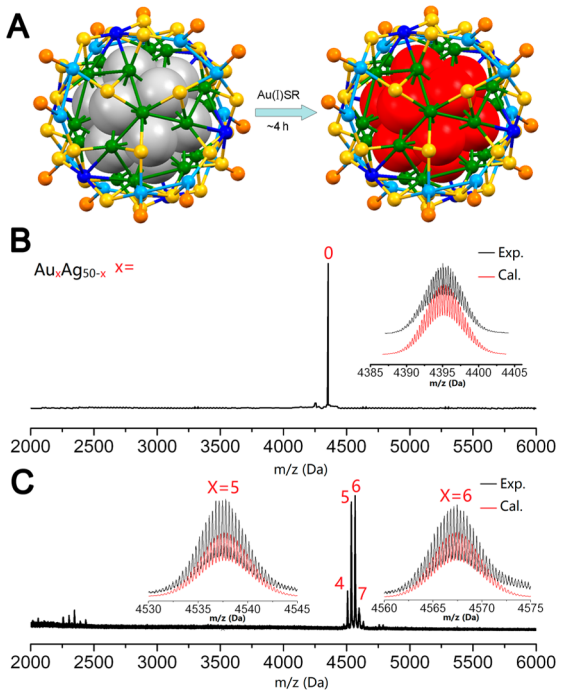

Figure 3. (A) Exchange from $Ag_{50}(Dppm)_6(TBBM)_{30}$ to $Au_xAg_{50-x}(Dppm)_6(TBBM)_{30}$ by a "templated/galvanic metal exchange" method. (B) ESI mass spectrum of $Ag_{50}(Dppm)_6(TBBM)_{30}$ NCs. Inset: experimental and simulated isotope patterns of $[Ag_{50}(Dppm)_6(TBBM)_{30} + 3Na^+ + K^+ - H^+]^{3+}$. (C) ESI mass spectrum of $Au_xAg_{50-x}(Dppm)_6(TBBM)_{30}$ NCs (x as indicated in each spectrum). Inset: experimental and simulated isotope patterns of $[Au_5Ag_{45}(Dppm)_6(TBBM)_{30} + 4Na^+ - H^+]^{3+}$ and $[Au_6Ag_{44}(Dppm)_6(TBBM)_{30} + 4Na^+ - H^+]^{3+}$. Color labels: gray/green/blue/sky blue = Ag; yellow = S; orange = P; red = Ag/Au.

silver atoms in the hollow M_{12} metal core. All the atoms in the M_{12} core were initially treated as partially occupied Au and Ag with the same coordinates and anisotropic displacement parameters, and the Au occupied atoms were converged to 44.5% (for details see, Figure S5).

The crystallographic data of these two clusters were similar (Table 1). As shown in Table 2, the doping of Au atoms made the average M−M bond (2.799 Å) in the M_{12} kernel a little shorter than that in the Ag_{50} (2.826 Å), and the average Ag−Ag bond in the Ag_{20} (3.194 Å) core was slightly larger than that in the undoped one (3.169 Å) (Figure S3). It was worth noting that the average Ag−S bond lengths in the center of the $Ag_{50}(Dppm)_6(SR)_{30}$ and $Au_{5.34}Ag_{44.66}(Dppm)_6(SR)_{30}$ clusters were in the range of 2.551−2.555 Å, which were shorter than other phosphine/thiol coprotected nanoclusters, such as $Ag_{14}(SC_6H_3F_2)_{12}(PPh_3)_8$ (2.612 Å).[64] The P−Ag bonds of the $Ag_{50}(Dppm)_6(SR)_{30}$ and $Au_{5.34}Ag_{44.66}(Dppm)_6(SR)_{30}$ clusters were also shorter than those of $Ag_{14}(SC_6H_3F_2)_{12}(PPh_3)_8$ by 1−2%.

As shown in Figure 3B, an intense peak was found at m/z 4395.19 Da. This peak and the isotope pattern analysis corresponded to those of $[Ag_{50}(Dppm)_6(TBBM)_{30} + 3Na^+ + K^+ - H^+]^{3+}$ (calculated m/z 4395.19 Da; Figure 3B inset). Similarly, two intense peaks at m/z 4537.44 and 4567.12 Da and two weak peaks at m/z 4507.79 and 4596.83 Da were revealed in Figure 3C. These peaks were assigned to $[Au_xAg_{50-x}(Dppm)_6(TBBM)_{30} + 4Na^+ - H^+]^{3+}$ (x = 4, 5, 6, 7) (calculated m/z 4507.79, 4537.44, 4567.14, and 4596.83 Da), confirmed by isotope pattern analysis (Figure 3C inset). From the peak height of the species, the average composition of the sample was found to be $Au_{5.42}Ag_{44.58}(Dppm)_6(SR)_{30}$, which was consistent with the single crystal data ($Au_{5.34}Ag_{44.66}(Dppm)_6(SR)_{30}$) (Table S1).

3.2. X-ray Photoelectron Spectroscopy. XPS results revealed that the atomic ratio was 10.89%/89.11% (Au/Ag, Table 3), which was consistent with the SCXRD result (Table 3). The XPS data was shown in Figure 4A, and details of data were shown in Figure S6. Figure S6C compared the Ag 3d spectra of $M_{5.34}Ag_{44.66}(Dppm)_6(SR)_{30}$ and bulk Ag. The Ag $3d_{5/2}$ peak of Ag_{50} nanocluster was at 368.42 eV and shifted to higher binding energies compared with that of bulk Ag (367.9 eV). This result illustrated that the valence state of Ag in the Ag_{50} nanocluster was positively charged. Following the inert gold doping into the metal core of Ag_{50} nanocluster, the Ag 3d spectra shifted away from the position of bulk silver, which suggested the valence state of silver was more positive than the homosilver nanocluster. The gold atoms were doped into the metal core of the silver nanocluster; it was reasonable that the gold was close to the metal form. As shown in Figure S6D, the Au $4f_{7/2}$ peak (84.3 eV) of $Au_{5.34}Ag_{44.66}$ nanocluster was close to the bulk Au $4f_{7/2}$ (84.0 eV).[65]

3.3. Optical Properties. The UV−vis absorption spectrum of $Ag_{50}(Dppm)_6(SR)_{30}$ in methanol at room temperature displayed three obvious peaks at ~415, 485, and 660 nm (Figure 4B). Meanwhile, $Au_{5.34}Ag_{44.66}(Dppm)_6(SR)_{30}$ displayed three obvious peaks at ~395, 485, and 616 nm. A significant change was that the 660 nm band moved to 616 nm by a 44 nm blueshift. The photon energy of HOMO−LUMO transition peak in Ag_{50} was 1.134 eV, which was lower than $Au_{5.34}Ag_{44.66}$ (1.235 eV) (Figure S7). This phenomenon might be due to Au heteroatom substitution, which increased the HOMO−LUMO energy gap (E_g) of nanocluster.[65] Obviously, the distinct difference of the optical absorption for $Au_{5.34}Ag_{44.66}(Dppm)_6(SR)_{30}$ and $Ag_{50}(Dppm)_6(SR)_{30}$ clusters indicated a significant contribution of the core metal atoms to the optical properties.

3.4. Photoluminescence Properties. As shown in Figure 4C, $Ag_{50}(Dppm)_6(SR)_{30}$ NCs exhibited inconspicuous photoluminescence. After doping gold atoms into this homosilver nanocluster, the obtained $Au_xAg_{50-x}(Dppm)_6(SR)_{30}$ exhibited an emission at the near-infrared region (870 nm). These dramatically enhancement together with the reported results suggested the gold doping was an efficient way to boost the photoluminescence intensity of homosilver nanocluster.[66,67]

3.5. Differential Pulse Voltammograms. Figure 4D illustrated differential pulse voltammograms (DPVs) of

Table 1. Summary of Crystallographic Data for $Ag_{50}(Dppm)_6(SR)_{30}$ and $Au_xAg_{50-x}(Dppm)_6(SR)_{30}$ Clusters

cluster composition[a]	space group	a (Å)	b (Å)	c (Å)	α (deg)	β (deg)	γ (deg)
$Ag_{50}(Dppm)_6(SR)_{30}$	$P\bar{1}$	26.2512(12)	26.6936(12)	26.7376(12)	76.576(2)	60.718(2)	61.726(2)
$Au_{5.34}Ag_{44.66}(Dppm)_6(SR)_{30}$	$P\bar{1}$	25.8780(9)	26.0327(9)	26.5129(9)	61.613(2)	75.949(2)	61.416(2)

[a]Dppm, bis(diphenylphosphino)methane; SR, 4-*tert*-butylbenzyl mercaptan.

DOI: 10.1021/jacs.6b11681
J. Am. Chem. Soc. 2017, 139, 1618−1624

Table 2. Summary of Important Average Bond Length Data for $Ag_{50}(Dppm)_6(SR)_{30}$ and $Au_xAg_{50-x}(Dppm)_6(SR)_{30}$ Clusters

cluster	M−M (Å)[a]	M−Ag (Å)[b]	Ag−Ag (Å)[c]	Ag−S (Å)[d]	Ag−S (Å)[e]	Ag−P (Å)[f]
$Ag_{50}(Dppm)_6(SR)_{30}$	2.826	2.861	3.169	2.551	2.638	2.447
$Au_{5.34}Ag_{44.66}(Dppm)_6(SR)_{30}$	2.799	2.861	3.194	2.555	2.630	2.464

[a]M−M bond length in the M_{12} shell (M = Au, Ag). [b]M−Ag bond length between the M_{12} and Ag_{20} shell. [c]Ag−Ag bond length in the Ag_{20} shell. [d]Ag−S bond length between the Ag and thiolate in the waist of the crystal. [e]Ag−S bond length between the Ag and thiolate in the bottom of the crystal. [f]Ag−P bond length between the Ag and phosphorus.

Table 3. Atom Ratio of Au/Ag Measured by XPS and SCXRD

	XPS experiment ratio	SCXRD ratio
Au atom	10.89% (5.44/50)	10.68% (5.34/50)
Ag atom	89.11% (44.56/50)	89.32% (44.66/50)

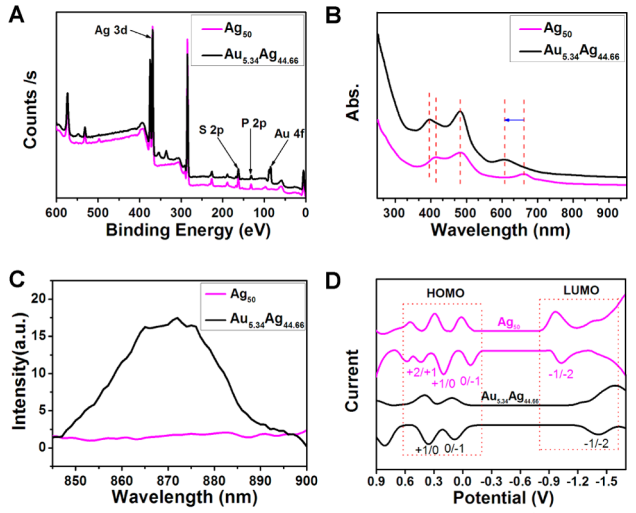

Figure 4. Comparison of $Ag_{50}(Dppm)_6(SR)_{30}$ (magenta line) and $Au_{5.34}Ag_{44.66}(Dppm)_6(SR)_{30}$ (black line) for (A) XPS, (B) UV−vis, and (C) PL spectras, and (D) DPVs.

$Ag_{50}(Dppm)_6(SR)_{30}$ and $Au_{5.34}Ag_{44.66}(Dppm)_6(SR)_{30}$ nanoclusters at −42 °C in 0.1 M Bu_4NPF_6/CH_2Cl_2. The peaks of the Ag_{50} were found at +0.44 (O3), +0.20 (O2), −0.08 (O1), and −1.03 V (R1) (Table 4). The electrochemical energy gap

Table 4. Formal Potential Spacing (ΔV) in the DPV Potential Scans for Two Analogous NCs Dissolved in CH_2Cl_2 (eV)

	O3	O2	O1	R1
$Ag_{50}(Dppm)_6(SR)_{30}$	0.44	0.20	−0.08	−1.03
$Au_{5.34}Ag_{44.66}(Dppm)_6(SR)_{30}$	0.82	0.36	0.09	−1.42

of 0.95 V (Ag_{50}) was determined from the difference between the oxidation O1 and reduction R1 potentials.[68] The electrochemical energy gap of $Au_{5.34}Ag_{44.66}(Dppm)_6(SR)_{30}$ was determined to be 1.51 V using the same method. The electrochemically determined larger HOMO−LUMO energy gap (E_g) for $Au_{5.34}Ag_{44.66}$ was consistent with the photoelectron spectroscopy analysis. The energy of LUMO orbital of the alloy nanocluster was higher than the homosilver nanocluster; a similar trend was also reported by Jin's and Zhu's groups.[65,69] Interestingly, the HOMO orbital of the alloy nanoclusters lower than the homosilver nanocluster, which was found for the first time, indicated that the gold doping could affect the HOMO orbital in the alloy nanoclusters. The lower HOMO orbital explained the higher stability of the alloy nanocluster.

3.6. DFT Calculations. Analysis of the local charge in metal atoms in the three shells 1 (kernel with 12 atoms), 2 (20 atoms), and 3 (18 atoms) was performed using the hirshfeld analysis method in Dmol^3 package, and the results were shown in Tables S3 and S4, from which we could see the change of the charge in the two clusters. For example, as shown in Table S3, the charge of the kernel with 12 metal atoms decreased from 0.098 to −0.077 after replacing six silver atoms with six gold atoms. In addition, compared with the Ag_{50} clusters, except with the corresponding Ag doped by gold atom, the charge of the rest of 44 Ag atoms increased by ∼0.162|e| (from +3.713 to +3.875), which was consistent with XPS analysis. Table S4 listed the Hirshfeld charge in the kernels of the two clusters in detail.

4. CONCLUSION

In summary, we have synthesized $Ag_{50}(Dppm)_6(SR)_{30}$ by seeded growth of $Ag_{44}(p\text{-MBA})_{30}$ nanocluster. This new nanocluster has been identified by X-ray diffraction and confirmed by ESI-MS and XPS. In order to further increase the stability of the homosilver Ag_{50} nanocluster, the templated/galvanic metal exchange method is carried out to exchange the core silver atoms with inert gold atoms. The obtained $Au_xAg_{50-x}(Dppm)_6(SR)_{30}$ nanocluster is also identified by X-ray diffraction and confirmed by ESI-MS and XPS. The optical, photoluminescence, electrochemical, and thermal stability experiments revealed that the doping of gold into the silver core can largely affect both HOMO and LUMO orbitals and increase the stability of homosilver nanoclusters. Our work will benefit better understanding on the synthesis of stable, large-size homosilver and silver-based alloy nanoclusters, as well as the structure related properties.

■ ASSOCIATED CONTENT

Supporting Information

The Supporting Information is available free of charge on the ACS Publications website at DOI: 10.1021/jacs.6b11681.

Details of structure analysis, thermal stability experiment, XPS, and DFT calculation (PDF)

Crystallographic information file for $Ag_{50}(Dppm)_6(SR)_{30}$ (CIF)

Crystallographic information file for $Au_{5.34}Ag_{44.66}(Dppm)_6(SR)_{30}$ (CIF)

■ AUTHOR INFORMATION

Corresponding Authors

*ixing@ahu.edu.cn

*zmz@ahu.edu.cn

ORCID

Yong Pei: 0000-0003-0585-2045

Shuxin Wang: 0000-0003-0403-3953

DOI: 10.1021/jacs.6b11681
J. Am. Chem. Soc. 2017, 139, 1618−1624

Manzhou Zhu: 0000-0002-3068-7160

Author Contributions

W.D. and S.J contributed equally to this work.

Notes

The authors declare no competing financial interest.

■ ACKNOWLEDGMENTS

We acknowledge financial support by NSFC (21372006, U1532141, and 21631001), the Ministry of Education, the Education Department of Anhui Province, 211 Project of Anhui University.

■ REFERENCES

(1) Price, R. C.; Whetten, R. L. *J. Am. Chem. Soc.* **2005**, *127*, 13750.
(2) Cathcart, N.; Mistry, P.; Makra, C.; Pietrobon, B.; Coombs, N.; Jelokhani-Niaraki, M.; Kitaev, V. *Langmuir* **2009**, *25*, 5840.
(3) Jin, R.; Zeng, C.; Zhou, M.; Chen, Y. *Chem. Rev.* **2016**, *116*, 10346.
(4) Joshi, C. P.; Bootharaju, M. S.; Bakr, O. M. *J. Phys. Chem. Lett.* **2015**, *6*, 3023.
(5) Jin, R. *Nanoscale* **2015**, *7*, 1549.
(6) Das, A.; Liu, C.; Byun, H. Y.; Nobusada, K.; Zhao, S.; Rosi, N.; Jin, R. *Angew. Chem.* **2015**, *127*, 3183.
(7) Chen, S.; Wang, S.; Zhong, J.; Song, Y.; Zhang, J.; Sheng, H.; Pei, Y.; Zhu, M. *Angew. Chem.* **2015**, *127*, 3188.
(8) Wan, X.; Lin, Z.; Wang, Q. *J. Am. Chem. Soc.* **2012**, *134*, 14750.
(9) Zeng, C.; Liu, C.; Chen, Y.; Rosi, N. L.; Jin, R. *J. Am. Chem. Soc.* **2014**, *136*, 11922.
(10) Chen, S.; Xiong, L.; Wang, S.; Ma, Z.; Jin, S.; Sheng, H.; Pei, Y.; Zhu, M. *J. Am. Chem. Soc.* **2016**, *138*, 10754.
(11) Chen, J.; Zhang, Q.; Bonaccorso, T. A.; Williard, P. G.; Wang, L. *J. Am. Chem. Soc.* **2014**, *136*, 92.
(12) Das, A.; Li, T.; Nobusada, K.; Zeng, C.; Rosi, N. L.; Jin, R. *J. Am. Chem. Soc.* **2013**, *135*, 18264.
(13) Das, A.; Li, T.; Li, G.; Nobusada, K.; Zeng, C.; Rosi, N. L.; Jin, R. *Nanoscale* **2014**, *6*, 6458.
(14) Song, Y.; Wang, S.; Zhang, J.; Kang, X.; Chen, S.; Li, P.; Sheng, H.; Zhu, M. *J. Am. Chem. Soc.* **2014**, *136*, 2963.
(15) Gan, Z.; Lin, Y.; Luo, L.; Han, G.; Liu, W.; Liu, Z.; Yao, C.; Weng, L.; Liao, L.; Chen, J.; Liu, X.; Luo, Y.; Wang, C.; Wei, S.; Wu, Z. *Angew. Chem.* **2016**, *128*, 11739.
(16) Zhu, M.; Aikens, C. M.; Hollander, F. J.; Schatz, G. C.; Jin, R. *J. Am. Chem. Soc.* **2008**, *130*, 5883.
(17) Heaven, M. W.; Dass, A.; White, P. S.; Holt, K. M.; Murray, R. W. *J. Am. Chem. Soc.* **2008**, *130*, 3754.
(18) Akola, J.; Walter, M.; Whetten, R. L.; Häkkinen, H.; Grönbeck, H. *J. Am. Chem. Soc.* **2008**, *130*, 3756.
(19) Zeng, C.; Chen, Y.; Iida, K.; Nobusada, K.; Kirschbaum, K.; Lambright, K. J.; Jin, R. *J. Am. Chem. Soc.* **2016**, *138*, 3950.
(20) Chen, Y.; Liu, C.; Tang, Q.; Zeng, C.; Higaki, T.; Das, A.; Jiang, D.; Rosi, N. L.; Jin, R. *J. Am. Chem. Soc.* **2016**, *138*, 1482.
(21) Zeng, C.; Li, T.; Das, A.; Rosi, N. L.; Jin, R. *J. Am. Chem. Soc.* **2013**, *135*, 10011.
(22) Dass, A.; Jones, T.; Rambukwella, M.; Crasto, D.; Gagnon, K. J.; Sementa, L.; De Vetta, M.; Baseggio, O.; Aprà, E.; Stener, M.; Fortunelli, A. *J. Phys. Chem. C* **2016**, *120*, 6256.
(23) Crasto, D.; Malola, S.; Brosofsky, G.; Dass, A.; Häkkinen, H. *J. Am. Chem. Soc.* **2014**, *136*, 5000.
(24) Das, A.; Liu, C.; Zeng, C.; Li, G.; Li, T.; Rosi, N. L.; Jin, R. *J. Phys. Chem. A* **2014**, *118*, 8264.
(25) Zeng, C.; Qian, H.; Li, T.; Li, G.; Rosi, N. L.; Yoon, N.; Barnett, R. N.; Whetten, R. L.; Landman, U.; Jin, R. *Angew. Chem., Int. Ed.* **2012**, *51*, 13114.
(26) Jin, R.; Liu, C.; Zhao, S.; Das, A.; Xing, H.; Gayathri, C.; Xing, Y.; Rosi, N. L.; Gil, R. R.; Jin, R. *ACS Nano* **2015**, *9*, 8530.
(27) Qian, H.; Eckenhoff, W. T.; Zhu, Y.; Pintauer, T.; Jin, R. *J. Am. Chem. Soc.* **2010**, *132*, 8280.
(28) Zeng, C.; Chen, Y.; Liu, C.; Nobusada, K.; Rosi, N. L.; Jin, R. *Sci. Adv.* **2015**, *1*, e1500425.
(29) Liao, L.; Zhuang, S.; Yao, C.; Yan, N.; Chen, J.; Wang, C.; Xia, N.; Liu, X.; Li, M.; Li, L.; Bao, X.; Wu, Z. *J. Am. Chem. Soc.* **2016**, *138*, 10425.
(30) Zeng, C.; Liu, C.; Chen, Y.; Rosi, N. L.; Jin, R. *J. Am. Chem. Soc.* **2016**, *138*, 8710.
(31) Jadzinsky, P. D.; Calero, G.; Ackerson, C. J.; Bushnell, D. A.; Kornberg, R. D. *Science* **2007**, *318*, 430.
(32) Salorinne, K.; Malola, S.; Wong, O. A.; Rithner, C. D.; Chen, X.; Ackerson, C. J.; Hakkinen, H. *Nat. Commun.* **2016**, *7*, 10401.
(33) Chen, Y.; Zeng, C.; Liu, C.; Kirschbaum, K.; Gayathri, C.; Gil, R. R.; Rosi, N. L.; Jin, R. *J. Am. Chem. Soc.* **2015**, *137*, 10076.
(34) Zeng, C.; Chen, Y.; Kirschbaum, K.; Appavoo, K.; Sfeir, M. Y.; Jin, R. *Sci. Adv.* **2015**, *1*, e1500045.
(35) Dass, A.; Theivendran, S.; Nimmala, P. R.; Kumara, C.; Jupally, V. R.; Fortunelli, A.; Sementa, L.; Barcaro, G.; Zuo, X.; Noll, B. C. *J. Am. Chem. Soc.* **2015**, *137*, 4610.
(36) Wallace, W. T.; Wyrwas, R. B.; Whetten, R. L.; Mitrić, R.; Bonačić-Koutecký, V. *J. Am. Chem. Soc.* **2003**, *125*, 8408.
(37) Negishi, Y.; Mizuno, M.; Hirayama, M.; Omatoi, M.; Takayama, T.; Iwase, A.; Kudo, A. *Nanoscale* **2013**, *5*, 7188.
(38) Urushizaki, M.; Kitazawa, H.; Takano, S.; Takahata, R.; Yamazoe, S.; Tsukuda, T. *J. Phys. Chem. C* **2015**, *119*, 27483.
(39) Kwak, K.; Kumar, S. S.; Pyo, K.; Lee, D. *ACS Nano* **2014**, *8*, 671.
(40) Tao, Y.; Li, M.; Ren, J.; Qu, X. *Chem. Soc. Rev.* **2015**, *44*, 8636.
(41) Zheng, K.; Yuan, X.; Goswami, N.; Zhang, Q.; Xie, J. *RSC Adv.* **2014**, *4*, 60581.
(42) Ghosh, A.; Udayabhaskararao, T.; Pradeep, T. *J. Phys. Chem. Lett.* **2012**, *3*, 1997.
(43) Li, G.; Lei, Z.; Wang, Q. M. *J. Am. Chem. Soc.* **2010**, *132*, 17678.
(44) Kang, X.; Wang, S.; Song, Y.; Jin, S.; Sun, G.; Yu, H.; Zhu, M. *Angew. Chem., Int. Ed.* **2016**, *55*, 3611.
(45) Wang, S.; Meng, X.; Das, A.; Li, T.; Song, Y.; Cao, T.; Zhu, X.; Zhu, M.; Jin, R. *Angew. Chem., Int. Ed.* **2014**, *53*, 2376.
(46) Yao, Q.; Yuan, X.; Yu, Y.; Yu, Y.; Xie, J.; Lee, J. Y. *J. Am. Chem. Soc.* **2015**, *137*, 2128.
(47) Zhu, M.; Aikens, C. M.; Hendrich, M. P.; Gupta, R.; Qian, H.; Schatz, G. C.; Jin, R. *J. Am. Chem. Soc.* **2009**, *131*, 2490.
(48) Antonello, S.; Perera, N. V.; Ruzzi, M.; Gascon, J. A.; Maran, F. *J. Am. Chem. Soc.* **2013**, *135*, 15585.
(49) Chen, Y.; Choi, H.; Kamat, P. V. *J. Am. Chem. Soc.* **2013**, *135*, 8822.
(50) Stamplecoskie, K. G.; Swint, A. *J. Mater. Chem. A* **2016**, *4*, 2075.
(51) Whetten, R. L.; Khoury, J. T.; Alvarez, M. M.; Murthy, S.; Vezmar, I.; Wang, Z. L.; Stephens, P. W.; Cleveland, C. L.; Luedtke, W. D.; Landman, U. *Adv. Mater.* **1996**, *8*, 428.
(52) Ingram, R. S.; Hostetler, M. J.; Murray, R. W. *J. Am. Chem. Soc.* **1997**, *119*, 9175.
(53) Song, Y.; Huang, T.; Murray, R. W. *J. Am. Chem. Soc.* **2003**, *125*, 11694.
(54) Shichibu, Y.; Negishi, Y.; Watanabe, T.; Chaki, N. K.; Kawaguchi, H.; Tsukuda, T. *J. Phys. Chem. C* **2007**, *111*, 7845.
(55) Bakr, O. M.; Amendola, V.; Aikens, C. M.; Wenseleers, W.; Li, R.; Dal Negro, L.; Schatz, G. C.; Stellacci, F. *Angew. Chem., Int. Ed.* **2009**, *48*, 5921.
(56) Harkness, K. M.; Tang, Y.; Dass, A.; Pan, J.; Kothalawala, N.; Reddy, V. J.; Cliffel, D. E.; Demeler, B.; Stellacci, F.; Bakr, O. M.; McLean, J. A. *Nanoscale* **2012**, *4*, 4269.
(57) Desireddy, A.; Guo, J.; Conn, B. E.; Yoon, B.; Barnett, R. N.; Monahan, B. M.; Kirschbaum, K.; Griffith, W. P.; Whetten, R. L.; Landman, U.; Bigioni, T. *Nature* **2013**, *501*, 399.
(58) Yang, H.; Wang, Y.; Huang, H.; Gell, L.; Lehtovaara, L.; Malola, S.; Häkkinen, H.; Zheng, N. *Nat. Commun.* **2013**, *4*, 2422.
(59) Wang, S.; Song, Y.; Jin, S.; Liu, X.; Zhang, J.; Pei, Y.; Meng, X.; Chen, M.; Li, P.; Zhu, M. *J. Am. Chem. Soc.* **2015**, *137*, 4018.
(60) Shon, Y. S.; Dawson, G. B.; Porter, M.; Murray, R. W. *Langmuir* **2002**, *18*, 3880.

DOI: 10.1021/jacs.6b11681
J. Am. Chem. Soc. 2017, 139, 1618−1624

(61) Perdew, J. P.; Burke, K.; Ernzerhof, M. *Phys. Rev. Lett.* **1996**, *77*, 3865.
(62) Delley, B. *J. Chem. Phys.* **1990**, *92*, 508.
(63) Delley, B. *J. Chem. Phys.* **2000**, *113*, 7756.
(64) Yang, H.; Lei, J.; Wu, B.; Wang, Y.; Zhou, M.; Xia, A.; Zheng, L.; Zheng, N. *Chem. Commun.* **2013**, *49*, 300.
(65) Kauffman, D. R.; Alfonso, D.; Matranga, C.; Qian, H.; Jin, R. *J. Phys. Chem. C* **2013**, *117*, 7914.
(66) Bootharaju, M. S.; Joshi, C. P.; Parida, M. R.; Mohammed, O. F.; Bakr, O. M. *Angew. Chem., Int. Ed.* **2016**, *55*, 824.
(67) Soldan, G.; Aljuhani, M.; Bootharaju, M. S.; Abdulhalim, L. G.; Parida, M. R.; Emwas, A.; Mohammed, O. F.; Bakr, O. M. *Angew. Chem., Int. Ed.* **2016**, *55*, 5749.
(68) Kwak, K.; Lee, D. *J. Phys. Chem. Lett.* **2012**, *3*, 2476.
(69) Kang, X.; Chen, S.; Jin, S.; Song, Y.; Xu, Y.; Yu, H.; Sheng, H.; Zhu, M. *ChemElectroChem* **2016**, *3*, 1261.
(70) Alhilaly, M. J.; Bootharaju, M. S.; Joshi, C. P.; Besong, T. M.; Emwas, A. H.; Juarez-Mosqueda, R.; Kaappa, S.; Malola, S.; Adil, K.; Shkurenko, A.; Hakkinen, H.; Eddaoudi, M.; Bakr, O. M. *J. Am. Chem. Soc.* **2016**, *138*, 14727.
(71) Yang, H.; Wang, Y.; Chen, X.; Zhao, X.; Gu, L.; Huang, H.; Yan, J.; Xu, C.; Li, G.; Wu, J.; Edwards, A. J.; Dittrich, B.; Tang, Z.; Wang, D.; Lehtovaara, L.; Hakkinen, H.; Zheng, N. *Nat. Commun.* **2016**, *7*, 12809.

NOTE ADDED IN PROOF

After we finished this work, we noted that two silver nanoclusters larger than Ag_{44} have been reported by Bakr's group[70] and Zheng's group,[71] respectively. Both of them are synthesized by direct method.

DOI: 10.1021/jacs.6b11681
J. Am. Chem. Soc. 2017, 139, 1618−1624